CHINA FOUNDRY Research & Development
Vol. 23 No. 6 November 2026
www.springer.com/41230
https://doi.org/10.1007/s41230-026-4205-7

Effect of position and height of liquid slag nozzle on steel-slag flow behavior in continuous casting mold

Lan Cui[1, 2], **Ye Zhou[1], Si-yao Liu[1], Qing-he Xiao[1], Hai-xiao Liu[1], Xin-gang Ai[1], Rui Guan[1], and *Sheng-li Li[1]

1. School of Materials and Metallurgy, University of Science and Technology Liaoning, Anshan 114051, Liaoning, China

2. Bengang Steel Plates Co., Ltd., Benxi 117100, Liaoning, China

Copyright © 2026 Foundry Journal Agency

Abstract: The reaction between Mn and Al in molten steel and SiO_2 in the protective slag generates MnO and Al_2O_3, which can cause drastic changes in the composition of the protective slag, deteriorate the quality of the casting billet, and hinder the continuous casting process. The present work proposed a new idea of adding low-reactive liquid protective slag to respond to this bottleneck. Both water model experiment and numerical simulation were carried out to investigate the influence of height and position of the slag nozzle on the flow behavior of liquid slag in the initial stage of continuous casting using a slab mold (1,050 mm×135 mm). The results show that the turbulence kinetic at the steel-slag interface is the largest when the slag nozzle height is set to 150 mm and its position is 131.25 mm away from the narrow face of the mold, and the variance value of liquid level height is 3.27×10^{-4}. This enhanced agitation is contributed to the flotation of inclusions and removal of bubbles in molten steel. At this time, the liquid slag spreading area is the largest, about 45.72%. When the height of the slag nozzle is set to 200 mm, the turbulence kinetic energy of the liquid surface generated by the steel-slag interface is the highest, and the corresponding variance value of the liquid level height is 3.69×10^{-4}. However, the variation of slag nozzle height has little effect on the ratio of liquid slag spreading area compared with the position of the slag nozzle.

Keywords: liquid slag nozzle; continuous casting mold; steel-slag flow behavior; water model; free surface fluctuation

CLC numbers: TG249.7 **Document code:** A **Article ID:** 1672-6421(2026)06-910-09

1 Introduction

High-manganese and high-alumina steel is extensively utilized in the metallurgy, aerospace, and automotive sectors owing to its superior wear resistance, high strength, and excellent corrosion resistance[1-3]. Nonetheless, during the continuous casting (CC) of slabs made from this steel, the high levels of reducing elements like Mn and Al in the molten metal can react with the SiO_2 in the $CaO\text{-}SiO_2\text{-}Al_2O_3$ ternary slag, leading to the replacement of silicon and the formation of various alloy oxides.

As the content of oxides in the alloy rises, the slag's basicity increases, adversely affecting its wettability, crystallization, and heat transfer characteristics. This deterioration can lead to significant slab surficial defects, such as indentations, cracks, and oscillation marks on CC slabs, thereby reducing production efficiency and heightening the risk of severe incidents like molten steel leakage. Thus, enhancing the performance stability of CC slag during steel-slag interactions is crucial for addressing the challenges of poor surface quality and production issues in high-manganese and high-alumina steel slab castings.

In actual production, it has been observed that the quality of the casting billet is most significantly influenced by the performance of the protective slag[4-6]. Recently, liquid protective slag has gained widespread attention due to its benefits, including reduced drawing force, improved lubrication, fewer vibration marks, and enhanced surface quality of the casting billet[7-8]. Gwon et al.[9] conducted production tests on liquid slag for continuous casting of TWIP steel, showing that alumina accumulation was 15%, which was 10% lower than that of conventional solid slag. However,

*Sheng-li Li
Male, born in 1967, Ph. D., Professor. Research interest: continuous casting.
E-mail: lishengliustl@163.com
**Ye Zhou
E-mail: zhouye@ustl.edu.cn
Received: 2024-09-22; Revised: 2024-12-23; Accepted: 2025-01-25

theoretical research on this topic is still at an early stage, and further investigation is required to fully understand its spreading, flow dynamics, infiltration, heat transfer, and other related behaviors.

The flow behavior of liquid slag within the mold is considered a crucial factor influencing the quality of CC slabs. The velocity of molten steel near the interface is influenced by both the thickness of the liquid slag layer and its properties. Key factors including the slag layer thickness and the shear velocity can impact the flow and heat transfer characteristics of the liquid slag layer[10-11]. Lu et al.[12] investigated the effects of various pouring parameters on the flow and heat transfer of liquid slag using the volume of fluid (VOF) model and a heat transfer model. Their findings revealed the presence of two recirculation zones of different sizes within the liquid slag layer over the molten steel in the mold's center plane, extending from the submerged entry nozzle (SEN) to the mold's narrow face. Zhang et al.[13] and Liu et al.[14] examined the movement of liquid slag at the meniscus and found that the mold experienced the alternating positive and negative slip states during the continuous casting process. This alternation led to periodic variations in the flow of liquid protective slag in the molten pool, both forward and reverse at the same time. Feldbauer[15] discovered that as the viscosity of the protective slag increased from 0.2 Pa·s to 0.5 Pa·s, the interfacial tension rose from 0.6 $N \cdot m^{-1}$ to 1.5 $N \cdot m^{-1}$. Additionally, the shear force exerted by the molten steel on the protective slag had minimal impact on the slag's flow, which helped reduce slag entrapment occurrences. Zhao et al.[16] investigated how temperature affects the viscosity of protective slag by developing a two-dimensional model of the liquid slag layer in the mold. They found that the change in Reynolds number with temperature mirrored that of the fluid with a constant viscosity. Du et al.[17] highlighted that the flow of molten steel significantly impacted the heat and flow transfer behavior of liquid slag, with conduction being the primary heat transfer mode when molten steel flow was considered. Furthermore, they observed that as the viscosity of the protective slag increased, the flow velocity of the slag layer decreased, leading to a marked reduction in heat transfer efficiency.

In recent years, numerous studies have focused on examining the fluctuations of liquid level in a CC mold[18]. It has been reported that variations in flow characteristics, including liquid level fluctuations, stimulus-response curves, liquid level velocity, and residue distribution, significantly influence fluid flow behavior within the mold[19]. Li et al.[20] employed the three-dimensional lattice Boltzmann method (LBM) to numerically simulate transient flow and liquid level fluctuations in the mold, revealing that the oscillatory behavior on both sides of the SEN plays a critical role in turbulence development. Cheng et al.[21] observed that argon blowing in the nozzle generated air bubbles that notably affected the flow and heat transfer behavior of the mold slag. They also identified a minor circulation of liquid slag in the central plane between the mold's wide face, near the side of the nozzle, and the mold's narrow face. Hu et al.[22] investigated the impact of solidification rate and pouring temperatures of liquid slag on the slag layer, providing a quantitative analysis of its spreading range and evolution, and discussed the uneven distribution and progression of the slag layer during the actual casting process. Zhang et al.[23] examined the liquid level fluctuations and slag entrainment behavior in the slab continuous casting mold, validating their simulation results with water model tests. They found that the fluctuations at the meniscus were more pronounced than those at the SEN. Liu et al.[24] demonstrated that the fluctuation of the steel-slag interface and the occurrence of slag entrapment diminished with an increased nozzle immersion depth. Deng et al.[25] highlighted that factors such as pulling velocity, SEN immersion depth, and tilt angle influenced the flow field and liquid level fluctuations in the mold. They noted that both nozzle inclination and larger tilt angle were unfavorable for the flotation of inclusions and bubbles, thus negatively impacting the quality of the casting billet.

In summary, liquid slag flow and liquid level fluctuations within the mold are critical factors influencing the quality of continuous casting billets. Few researchers have conducted the investigations on liquid protective slag and its interface flow behavior with molten steel. Therefore, this study aimed to investigate how the position and height of the liquid slag SEN affects the steel-slag flow behavior in the CC mold, using a combination of water model experiments and numerical simulations. The findings from this study were expected to be a theoretical support for the practical application of liquid slag in CC process.

2 Experimental method and numerical simulation

2.1 Numerical simulation

2.1.1 Physical properties and assumptions

The physical properties of molten steel and the CC process parameters utilized in this study are detailed in Tables 1 and 2. The assumptions for the model are as follows:

(1) The influence of the meniscus on liquid protective slag flow was ignored.

(2) Both the molten steel and the liquid protective slag within the mold were regarded as incompressible fluids and treated as homogeneous substances.

(3) The effects of the solidified shell and mold vibration on the flow behavior of the liquid slag were neglected.

(4) The loss of liquid slag was neglected.

2.1.2 Geometric model

A half of mold model (525 mm×135 mm) was established, assuming symmetry in the flow field inside the mold during the numerical calculations. Non-structural tetrahedral and hexahedral elements were used to divide the mesh, resulting

Table 1: Physical parameters of molten steel

Molten steel	Value	Liquid slag	Value
Density (kg·m^{-3})	7,000	Density (kg·m^{-3})	2,600
Specific heat [J·(kg·K)$^{-1}$]	720	Specific heat [J·(kg·K)$^{-1}$]	1,200
Thermal conductivity [W·(m·K)$^{-1}$]	31	Thermal conductivity [W·(m·K)$^{-1}$]	0.3
Viscosity (Pa·s)	0.0065	Solidus temperature (K)	1,307
Latent heat (J·kg^{-1})	275,000	Liquidus temperature (K)	1,486
Solidus temperature (K)	1,724	Interfacial tension between molten steel and slag (N·m^{-1})	1.058
Liquidus temperature (K)	1,970		

Table 2: CC process parameters

Parameters	Value
Cross-section of mold (mm×mm)	1,050×135
Outer SEN (mm×mm)	167×85
Dip angle of SEN (°)	15
Immersion degree of SEN (mm)	180
Flux of liquid slag (m^3·h^{-1})	10.22
Casting velocity (m·min^{-1})	1.2
Height of liquid slag SEN (mm)	100, 150, 200
Distance between liquid slag SEN and narrow face of mold (mm)	131.25, 262.50, 393.75

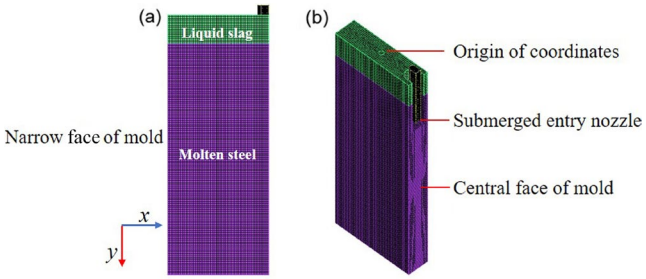


Fig. 1: Model meshing

in a total of 400,000 elements, as shown in Fig. 1. The SENs of the mold and the liquid slag were defined as velocity inlets in the boundary conditions. The walls were set as no-slip wall, and the standard wall function was applied to perform the flow behavior near the walls.

2.2 Water model experiment

In this section, the accuracy of the mathematical results was validated through water model experiments. The impact of varying liquid slag SEN positions and heights on the flow field, surface velocity, and slag distribution within the mold were studied during the initial stage of continuous casting. To ensure the reliability of the numerical simulations, the simulation outcomes were compared with the experimental results from the water model.

2.2.1 Physical model

A water model experiment was conducted to visualize the flow field, based on the principle of similarity. The physical model replaced the walls of the continuous casting mold with transparent plexiglass, and high-temperature molten steel was substituted with water, as the kinematic viscosity of molten steel at 1,600 °C is equivalent to that of water at 20 °C. This study primarily focused on achieving geometric and dynamic similarity, as meeting these criteria ensures the highest level of motion similarity between the model and the prototype.

It is important to note that geometric similarity requires a consistent scale between the physical model and the actual prototype. In the laboratory, the narrow face length of the mold was fixed. To conserve time and resources, the mold width was adjusted to meet the conditions necessary for geometric similarity.

In the CC process, the flow field within the mold was characterized by jet flow within a confined space, where the molten steel impacted the mold walls, creating turbulence in both the upper and lower recirculation zones. The primary factors influencing this turbulence are inertia and gravity. To ensure that the motion of the model accurately reflects that of the prototype, it is essential to match the Froude number (Fr) and Reynolds number (Re) between the model and the prototype.

Based on the equality of the Froude criteria, the model flow rate can be determined as follows:

$$(Fr)_r=(Fr)_m \quad (1)$$

$$u_m^2/(gL_m)=u_r^2/(gL_r) \quad (2)$$

$$u_m/u_r=L_m^{1/2}/L_r^{1/2}=\lambda^{1/2} \quad (3)$$

$$Q_m/Q_r=(u_mL_m^2)/(u_rL_r^2)=\lambda^{5/2} \quad (4)$$

$$Q_m=Q_r\times\lambda^{5/2} \quad (5)$$

where λ is the scale factor, r represents the prototype, and m represents the water model. u represents the velocity of fluid, and Q represents the flux through the cross-section, respectively.

2.2.2 Experimental equipment

A 1.4:1 scale model was employed in the experiment. The equipment used included a video camera, a light source, a water supply system, an LGY-6 multi-channel wave altimeter, a signal-receiving device, computer processing software, and the potassium permanganate as a tracer. The flow field distribution within the mold was captured under various process parameters, and the wave height meter recorded the liquid level fluctuations in the mold for different conditions by wave altimeter. Figure 2 illustrates the device setup for the water-model experiment. During the experiment, the mold was segmented into eight parts, and sensors measured the liquid level fluctuations at 1/8 away from the narrow surface center and 1/4 positions away from wide surface of the mold, respectively. The collected liquid level fluctuation data were processed using Data Management software. After adding potassium permanganate from the SEN, the tracer moved into the mold with the water flow, striking the narrow side of the mold along the flow stream. This setup allowed for the visualization of the flow field within the mold and provided valuable data to support the numerical simulations.

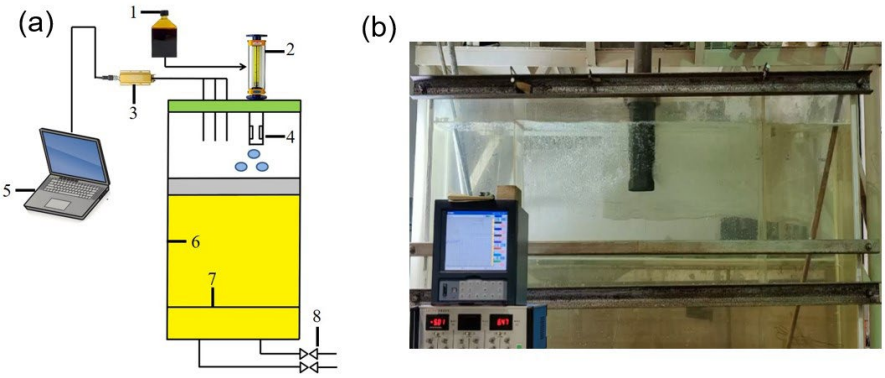


Fig. 2: Schematic diagram (a) and device diagram (b) of water model experiment (1-Tracer, 2-Flowmeter, 3-Wave altimeter, 4-SEN, 5-Computer, 6-Mold, 7-Slow-flow device, 8-Valve)

3 Results

3.1 Model verification

Figure 3 presents the results from the water model experiments alongside the velocity field and streamline diagrams at the center of the mold's wide face, as determined by numerical simulation. The results clearly demonstrate that the molten steel flow exhibits a jet pattern within a certain range, exiting through the side hole of the SEN and moving in a straight line toward the mold's narrow face. As the molten steel travels, it gradually disperses and splits into upper and lower streams due to tangential viscous force upon reaching the mold's narrow face.

In this process, the upper strand moves upward along the narrow face of the mold towards the free liquid surface, pushing molten steel toward the SEN. Simultaneously, the molten steel ejected from the SEN's side hole sweeps the surrounding flow in the direction of the main strand, creating a recirculation zone in the upper region of the mold. The fluctuated movement of molten steel within this upper recirculation zone is driven by fluctuations of the free liquid surface, which helps transport high-temperature molten steel to the free surface, facilitating the melting of the solid protective slag. Additionally, the upper recirculation zone significantly influences the flotation of inclusions in the molten steel: as the upward velocity of molten steel in the upper strand increases, the flotation rate of inclusions is enhanced.

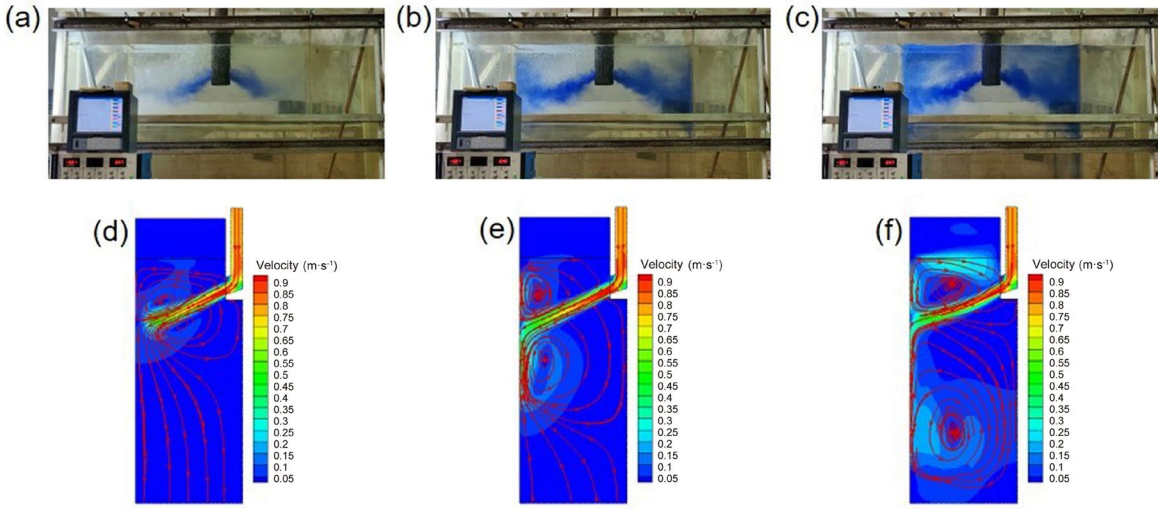


Fig. 3: Flow field in the mold of water model experiment (a, b, c) and mathematical simulation (d, e, f) of flow field in the center of wide surface of mold: (a and d) 5 s; (b and e) 10 s; (c and f) 30 s

3.2 Flow field of molten steel

Figure 4 displays a streamline diagram of the center velocity at the wide face of the mold when the slag SEN height is set to 150 mm, with corresponding positions away from the narrow face of mold at 131.25 mm (Position A), 262.50 mm (Position B), and 393.75 mm (Position C). It is important to note that the flow velocity and distribution patterns of molten steel are similar across the different conditions. At Position A, the velocity of the liquid protective slag increases as it interacts with the free liquid surface, reaching a maximum speed of 1.5 $m \cdot s^{-1}$. In contrast, at Positions B and C, the maximum velocity is observed to be 1.4 $m \cdot s^{-1}$.

Figures 4(d–f) depict the velocity and streamline patterns of molen steel at the center of the mold's wide side with the slag SEN positioned at A, at heights of 100 mm (H_1), 150 mm (H_2), and 200 mm (H_3). The flow field distribution and velocity within the molten steel remain consistent, with two recirculation zones appearing in the mold that are identical in size and location. However, the velocity of the liquid protective slag shows notable changes when it interacts with the free liquid surface. As the SEN height increases, the velocity of the liquid slag rises progressively, reaching maximum speeds of 1.1 $m \cdot s^{-1}$, 1.4 $m \cdot s^{-1}$, and 1.7 $m \cdot s^{-1}$ for H_1, H_2, and H_3, respectively, increasing the molten steel velocity near the impact point. This effect is attributed to the increased height of the slag SEN, which results in higher gravitational potential energy of the liquid slag, thereby enhancing its velocity.

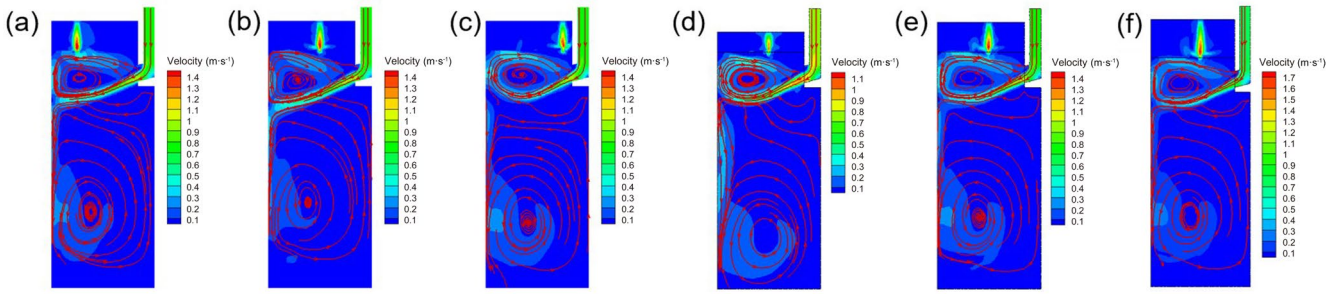


Fig. 4: Velocity contour and streamline diagram of wide-surface center of mold at different positions: (a) Position A; (b) Position B; (c) Position C; and wide-surface center of mold under different slag SEN heights: (d) H_1; (e) H_2; (f) H_3

3.3 Surface velocity of molten steel

Figure 5(a) illustrates the velocity distribution curve of the free liquid surface at the center of the mold's wide face when the slag SEN is positioned at various locations. It is observed that as the slag SEN moves closer to the molten steel SEN, the velocity of the free liquid surface initially decreases and then increases. When the slag SEN was positioned at 131.25 mm, 262.50 mm, and 393.75 mm from the narrow face of mold, the maximum velocities at the liquid slag impact point are 0.73, 0.71, and 0.97 $m \cdot s^{-1}$, respectively. The velocity at Position A is approximately equal to that at Position B. At Position B, the velocity near the slag SEN is lower than the surface flow velocity of molten steel around Position C, indicating that the influence zone of the upper recirculation region is smaller at Position B than at Position C. At Position C, the residual waves of the liquid slag flow field, after interacting with the free liquid surface, rebound upon encountering the wall of the molten steel SEN, leading to a noticeable enhancement of the velocity field of the molten steel in this region.

Figure 5(b) shows the velocity distribution of the free liquid surface at the center of the wide face as the SEN is positioned at A, but with different heights. As the SEN height increases, the overall velocity of the free liquid surface also exhibits an upward trend. The maximum velocities in the upper recirculation zone are 0.16, 0.18, and 0.22 $m \cdot s^{-1}$ for SEN heights of H_1, H_2, and H_3, respectively. Similarly, the maximum velocities at the liquid slag impact point are 0.54, 0.56, and 0.58 $m \cdot s^{-1}$. The velocity of the free liquid surface near the SEN area also rises with increasing SEN height. This indicates that as the SEN height increases, the gravitational potential energy of the liquid slag is converted into greater kinetic energy, resulting in a higher energy and impact force when the slag contacts the free liquid surface, thereby increasing the overall velocity of the free liquid surface.

3.4 Turbulent kinetic energy on free surface

Figures 6(a–c) show the turbulent kinetic energy distribution of the free liquid surface at various slag SEN positions. As the slag SEN position moves closer to the side of the SEN, the kinetic energy on the free liquid surface generally exhibits a decreasing trend. It is noteworthy that at Position A, a significant spike in kinetic energy is observed, while Positions B and C display two such peaks. The increase in kinetic energy around the slag SEN positions is attributed to the interaction of the two phases during the slag dripping process, which enhances the kinetic energy of the free liquid surface near the impact point. At Position A, the landing point of the liquid slag overlaps with the upper recirculation zone of the molten steel, resulting in more intense changes in the kinetic energy due to the two-phase mixing. The pulsating velocity generated in this mixing process is greater at Position A than that at the other positions, leading to the higher kinetic energy in this region compared to Positions B and C.

Figures 6(d–f) illustrate the turbulent kinetic energy distribution of the free liquid surface at varying heights of the slag filling port. Two high-energy regions are observed on the free liquid surface: one near the narrow face of the

mold and the other around the liquid slag impact point. As the height of the slag inlet increases, the kinetic energy of the free liquid surface also rises, with the most pronounced increase occurring around the slag drop point. This increase is due to the higher velocity of liquid slag dripping from greater SEN heights, which raises the impact energy when the slag contacts the free liquid surface, thereby boosting the kinetic energy around the drop point. When the high-speed liquid slag strikes the free liquid surface, the resulting residual waves disperses outward, carrying significant energy. Additionally, when the upper recirculation zone of the molten steel interacts with the free liquid surface, the impact between the two phases is intensified, resulting in even greater kinetic energy in these regions.

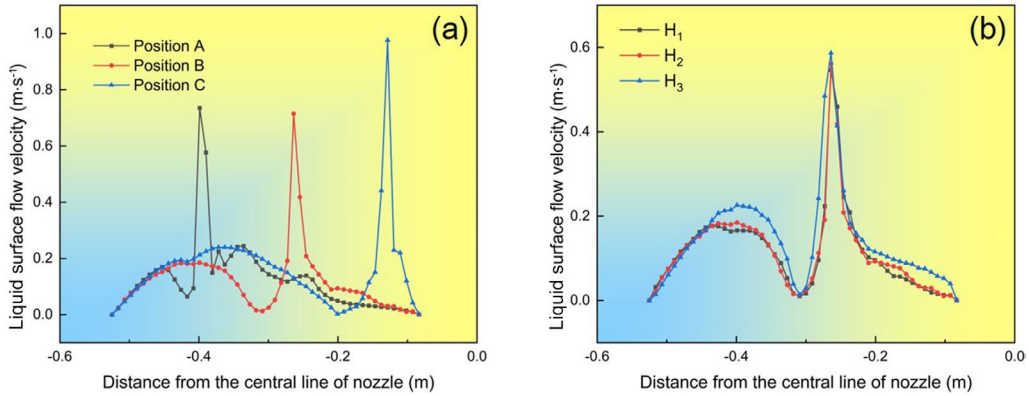


Fig. 5: Free surface velocity under different SEN positions (a) and heights (b)

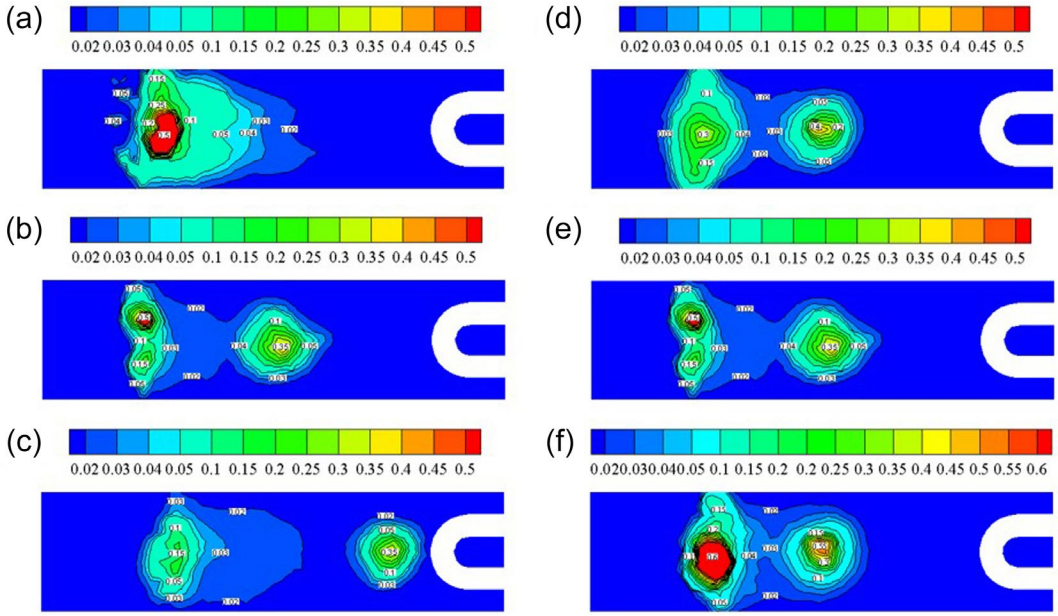


Fig. 6: Turbulent kinetic energy of free liquid surface under different slag SEN positions: (a) Position A; (b) Position B; (c) Position C; (d) H_1; (e) H_2; (f) H_3

4 Discussion

4.1 Influence of slag SEN position on liquid slag surface morphology and slag spreading behavior

The different positions of slag SEN influence the turbulent kinetic energy of the free liquid surface, which affects the fluctuation of the liquid level in turn. The fluctuations of free liquid slag surface level are recorded by multi-channel wave altimeter. Figures 7(a–c) depicts how the slag SEN position impacts the fluctuation of the free liquid surface at various locations, while Fig. 7(d) shows the variance in the height fluctuations of the liquid level at the center of the mold's wide side for different slag SEN positions. From Figs. 6(a–c) and 7, it is evident that as the slag SEN moves closer to the narrow face of the mold, the turbulent kinetic energy and the fluctuation intensity of the liquid surface increase. This enhanced fluctuation is beneficial for the flotation of inclusions and the removal of bubbles from the molten steel.

When the SEN was positioned at Position A (Fig. 7), only one trough appears on the liquid slag surface, with the liquid level height near the narrow face of the mold reaching 1.2 m and the corresponding variance of liquid level fluctuation being 3.27×10^{-4}. In contrast, when the SEN was positioned farther from the narrow face (Positions B and C), two troughs are observed on the liquid slag surface, and the variance of the

liquid level fluctuation decreases to 3.09×10^{-4} and 2.48×10^{-4}, respectively. It is important to note that the closer the slag SEN is to the narrow side of the mold, the more significantly the recirculation zone affects the flow of molten steel and liquid protective slag, leading to increased liquid level fluctuations. As the SEN position moves away from the narrow side of the mold, the variance in liquid level height decreases progressively from 3.27×10^{-4} to 2.48×10^{-4}, and the fluctuation of the liquid level diminishes accordingly. These results indicate that adjusting the slag SEN position nearer to the narrow side of the mold enhances the flotation of inclusions and aids in bubble removal from the molten steel, ultimately improving the quality of the continuous casting billet.

Figures 8 and 9 show the volume fraction of liquid slag at the center of the wide face of the mold for different nozzle positions and the corresponding exposed areas of molten steel, respectively. Figures 8 and 9 indicate that as the slag-filling SEN moves closer to the side of the SEN, the exposed area of molten steel increases. Compared to Positions B and C, when the slag-filling SEN is positioned at A, the molten steel surface has the smallest exposed area, and the slag coverage is at its maximum.

When the slag SEN was positioned at A, the flow of liquid slag significantly impacts the upper recirculation zone, with the slag droplets moving along with the molten steel's return flow toward the SEN. This causes the drop point to be exposed, allowing the slag to spread along the flow field in the upper region of the SEN, thereby increasing the slag coverage

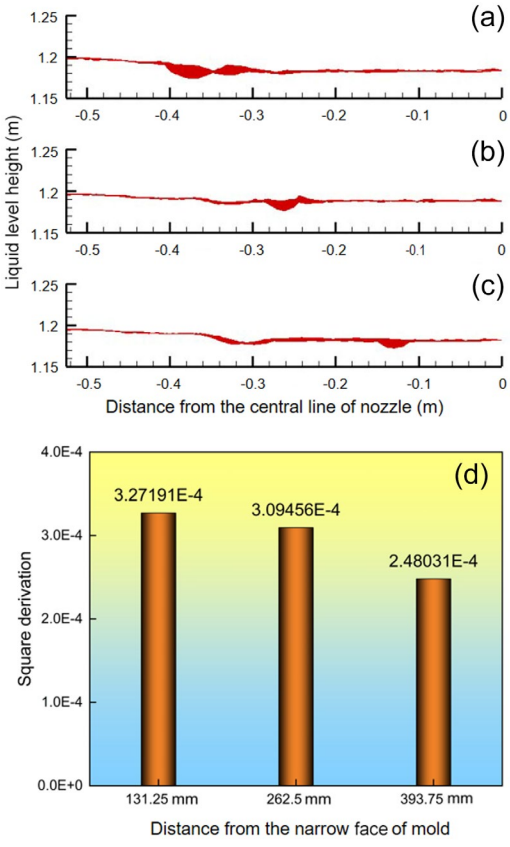


Fig. 7: Liquid slag surface morphology under different slag SEN positions: (a) Position A; (b) Position B; (c) Position C; (d) fluctuate square derivation

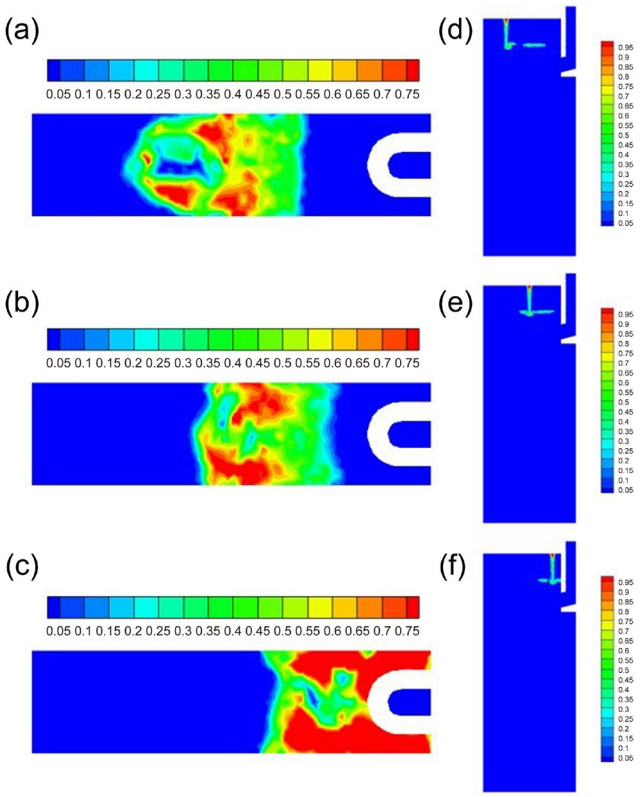


Fig. 8: Slag volume fraction on free surface and exposed area of molten steel of different slag filling SEN positions: (a and d) Position A; (b and e) Position B; (c and f) Position C

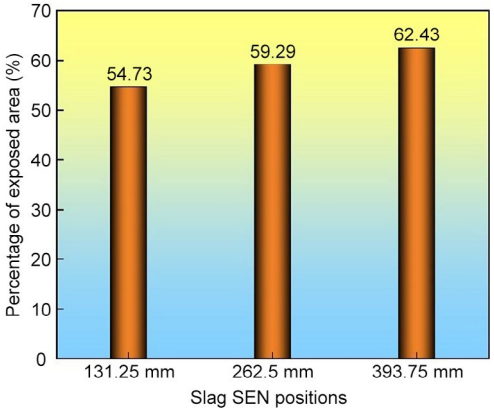


Fig. 9: Exposed area statistics of molten steel under different slag SEN positions

area. However, as the slag SEN moves closer to the molten steel nozzle, the liquid slag is positioned further away from the upper recirculation zone, and the influence of the molten steel flow field near the slag SEN diminishes. This reduction in flow intensity near the slag drop point results in the accumulation of slag, preventing it from spreading to other areas. Consequently, the coverage of the steel surface by the liquid slag decreases, leading to an increased cooling rate of molten steel.

4.2 Effect of slag SEN height on liquid slag surface morphology and slag spreading behavior

Figure 10 illustrates the impact of the slag SEN on the fluctuation intensity of the free liquid slag surface at various

heights, as well as the variance in liquid level height across the wide surface of the mold for different slag nozzle heights at Position B. It can be observed that the liquid level height near the SEN is lower compared to that near the mold's narrow face. This difference is owing to the formation of a recirculation zone by the steel liquid jet near the narrow face, which significantly influences the fluctuations of the free liquid slag level, causing it to rise near the mold's narrow face. As the height of the slag SEN increases, the free liquid level at the slag impact zone decreases, with trough liquid level heights measured at 1.18, 1.175, and 1.169 m, respectively.

The variance in liquid level height increases gradually from 2.08×10^{-4} to 3.69×10^{-4} as the slag SEN height increases from 100 to 200 mm, leading to more pronounced fluctuations in the free liquid level. Raising the height of the slag inlet boosts the gravitational potential energy of the liquid slag, causing it to impact the free surface at higher speeds and produce more fluctuation. This results in deeper penetration of the liquid slag into the steel, intensifying the disturbance at the liquid slag surface and promoting the flotation of inclusions.

Figures 11 and 12 display the schematic diagram of the liquid slag volume fraction at the center of the wide side and the statistics of the exposed area of molten steel at different SEN heights. As the height of the slag nozzle increases, the exposed area of the molten steel also increases. At nozzle heights H_2 and H_3, exposed areas of molten steel are observed at the liquid slag impact point. This occurs because, with increased height, the liquid slag exerts a greater impact on the steel surface, reducing the thickness of the slag layer near the impact point. Consequently, the steel in this region becomes more easily exposed, leading to a higher degree of oxidation.

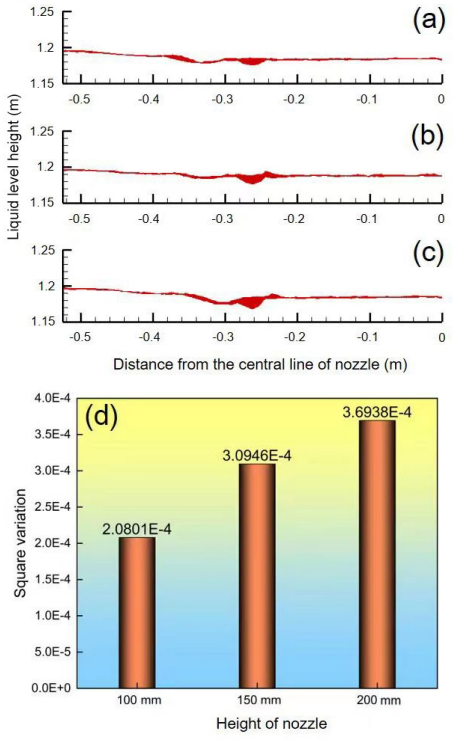


Fig. 10: Liquid slag surface morphology and variance of free liquid surface height under different slag SEN heights: (a) H_1; (b) H_2; (c) H_3

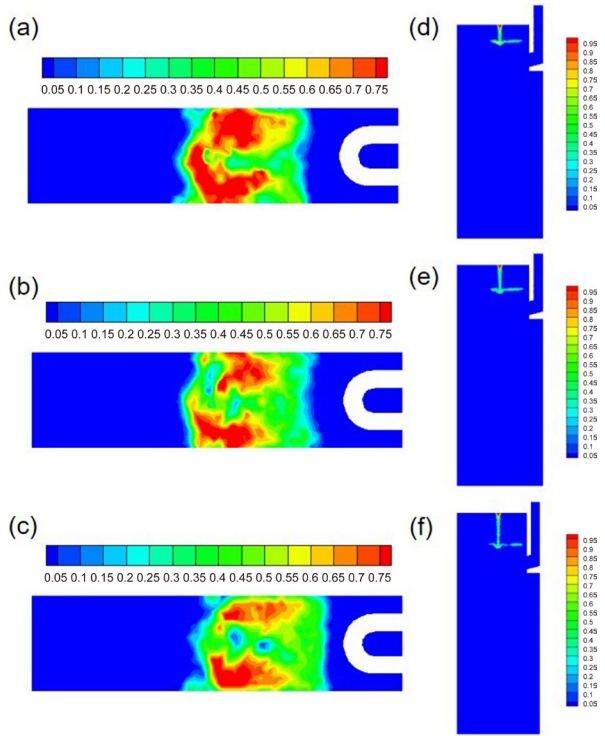


Fig. 11: Volume fraction of liquid slag at free liquid surface and volume fraction of liquid slag in the center of wide surface at different slag SEN heights: (a and d) H_1; (b and e) H_2; (c and f) H_3

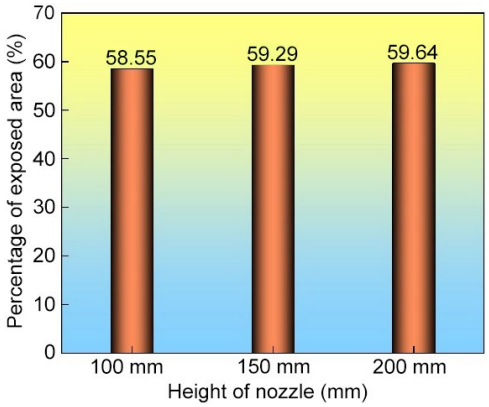


Fig. 12: Exposed area statistics of molten steel under different slag SEN heights

5 Conclusions

In this study, the impacts of various slag SEN heights and positions on the flow field of liquid slag and molten steel in the mold were investigated using a combination of water model experiments and numerical simulations. The key conclusions are as follows:

(1) As the liquid slag SEN moves to the side of the immersed SEN, the surface velocity shows a trend of first decreasing and then increasing. When the slag SEN is 131.25 mm away from the narrow surface of the mold, the flow velocity of molten metal reaches the maximum, 0.97 $m\cdot s^{-1}$. At the same time, the free surface turbulence kinetic energy at the molten steel-slag interface reaches the maximum, and the liquid level height variance value is 3.27×10^{-4}, which is conducive to the flotation of inclusions and the removal of bubbles in the molten steel.

(2) When the slag SEN height is set to 150 mm and positioned at 131.25 mm away from the narrow face of the mold, the liquid slag spreading area is the largest, about 45.72%, which is larger than the liquid slag spreading area when the slag SEN is 262.50 mm and 393.75 mm away from the narrow side of the mold.

(3) When the height of the slag SEN is set to 200 mm and positioned at 262.50 mm from the narrow face of mold, the turbulence kinetic energy generated by the free liquid surface is the largest, and the variance value of the liquid level height is 3.69×10^{-4}, which is conducive to the flotation of inclusions in the molten steel and the removal of bubbles.

Acknowledgments

The authors would like to acknowledge the National Natural Science Foundation of China (51974155), the Outstanding Young Scientific and Technological Talents Project of University of Science and Technology Liaoning (2023YQ07), the Project supported by the Natural Science Foundation of Liaoning Province (2024-BS-221), the National Key Research and Development Program (2021YFB3702005), the Central Government Guides Local Science and Technology Development Fund Projects (2023JH6/100100046), and the Liaoning Provincial Department of Education Basic Research Projects for Universities (JYTQN2023242).

Conflict of interest

The authors declare that they have no known competing financial interests or personal relationships that could have appeared to influence the work reported in this paper.

References

[1] Mahapatra R B, Brimacombe J K, Samarasekera I V, et al. Mold behavior and its influence on quality in the continuous casting of steel slabs: Part i. Industrial trials, mold temperature measurements, and mathematical modeling. Metall. Mater. Trans. B, 1991, 22: 861–874.
[2] Anisimov K N, Longinov A M, Toptygin A M, et al. Investigation of the mold powder film structure and its influence on the developed surface in continuous casting. Steel Transl., 2016, 46(7): 489–495.
[3] Lu H B, Cheng C G, Li Y, et al. Flow and heat transfer of liquid slag in a continuous casting mold. J. Iron Steel Res. Int., 2019, 26: 926–940.
[4] Thomas B G. Modeling of the continuous casting of steel-past, present, and future. Metall. Mater. Trans. B, 2002, 33: 795–812.
[5] Guthrie R I and Isac M M. Continuous casting practices for steel: Past, present and future. Metals, 2022, 12(5): 862.
[6] Lozovskii E P, Alekseev A G, Yurechko D V, et al. In-house produced slag-forming mixtures in the continuous-casting machine in the oxygen-converter plant and the electric arc furnace shop: Development and usage. Steel Transl., 2021, 51: 39–41.
[7] Yan W, Yang Y D, Chen W Q, et al. Design of mould fluxes for continuous casting of special steels. Can. Metall. Q., 2015, 54(4): 467–476.
[8] Cho J W, Yoo S, Park M S, et al. Improvement of castability and surface quality of continuously cast TWIP slabs by molten mold flux feeding technology. Metall. Mater. Trans. B, 2017, 48: 1–10.
[9] Gwon H J, Shin S M, Jeon J B, et al. Hot deformation behavior of V micro-alloyed TWIP steel during hot compression. Met. Mater. Int., 2019, 25: 594–605.
[10] Nakada H, Susa M, Seko Y, et al. Mechanism of heat transfer reduction by crystallization of mold flux for continuous casting. ISIJ Int., 2008, 48(4): 446–453.
[11] Scheller P R. Interfacial phenomena between fluxes for continuous casting and liquid stainless steel. Ironmaking Steelmaking, 2002, 29(2): 154–160.
[12] Li G H, Wang S J, and Zheng G T. Flow and heat transfer on the surface of molten steel slag layer in continuous casting mold. Coatings, 2023, 13(9): 1551.
[13] Zhang X B, Chen W, and Zhang L F. A coupled model on fluid flow, heat transfer and solidification in continuous casting mold. China Foundry, 2017, 14(5): 416–420.
[14] Liu J G, Yan H C, Liu L, et al. Water modeling of optimizing tundish flow field. J. Iron Steel Res. Int., 2007, 14(3): 13–19.
[15] Feldbauer S L. Slag entrainment in the mold of a continuous caster. Doctoral Dissertation, Carnegie Mellon University, USA, 1995.
[16] Zhao B, Vanka S P, and Thomas B G. Numerical study of flow and heat transfer in a molten flux layer. Int. J. Heat Fluid Flow, 2005, 26(1): 105–118.
[17] Du F M, Zeng Y B, Wang S J, et al. Analysis of flow and fluctuation characteristics in coated slag using a 2D model in the meniscus region of mold. Coatings, 2023, 13(10): 1678.
[18] He Y B, Zhou H L, Zhang B Q, et al. Prediction model of liquid level fluctuation in continuous casting mold based on GA-CNN. Metall. Mater. Trans. B, 2024, 55(3): 1414–1427.
[19] Shen B, Shen H, and Liu B. Instability of fluid flow and level fluctuation in continuous thin slab casting mould. ISIJ Int., 2007, 47(3): 427–432.
[20] Li Q. Repetitive control with feedforward scheme for periodic vibration displacement control of mold driven by servo motor. CEAI, 2024, 26(2): 25–35.
[21] Cheng C G, Lu H B, Li Y, et al. Mathematical modeling of flow and heat transfer behavior of liquid slag in continuous casting mold with argon blowing. ISIJ Int., 2019, 59(7): 1266–1275.
[22] Hu P H, Wang X D, Wei J J, et al. Investigation of liquid/solid slag and air gap behavior inside the mold during continuous slab casting. ISIJ Int., 2018, 58(5): 892–898.
[23] Zhang H H and Wang W L. Mold simulator study of the initial solidification of molten steel in continuous casting mold: Part II. Effects of mold oscillation and mold level fluctuation. Metall. Mater. Trans. B, 2016, 47: 920–931.
[24] Liu Y B, Yang J, Huang F X, et al. Comparison of the flow field in a slab continuous casting mold between the thicknesses of 180 mm and 250 mm by high temperature quantitative measurement and numerical simulation. Metals, 2021, 11(12): 1886.
[25] Deng A Y, Xu L, Wang E G, et al. Numerical analysis of fluctuation behavior of steel/slag interface in continuous casting mold with static magnetic field. J. Iron Steel Res. Int., 2014, 21(9): 809–816.